Electronic Supplementary Material (ESI) for Dalton Transactions.

Electronic Supplementary Information (ESI)

Anion-Mediated Encapsulation-Induced Emission Enhancement of an Ir^{III} Complex within a Resorcin[4]arene Hexameric Capsule

Shinnosuke Horiuchi,*[a,,b] Chiharu Matsuo,[a] Eri Sakuda,[a,b] Yasuhiro Arikawa,[a] Guido H. Clever,[b] and Keisuke Umakoshi*[a]

E-mail: shoriuchi@nagasaki-u.ac.jp, kumks@nagasaki-u.ac.jp

[a] Division of Chemistry and Materials Science, Graduate School of Engineering, Nagasaki University, Bunkyo-machi, Nagasaki, 852-8521 Japan

[b] Faculty of Chemistry and Chemical Biology, TU Dortmund University, Otto-Hahn-Strasse 6, 44227, Dortmund, Germany

Contents

Materials and Instrumentations

The ^{1}H, ^{19}F and DOSY NMR spectra were obtained at 300 MHz with a Varian Gemini 300 and 500 MHz (470 MHz for ^{19}F) with Varian NMR System 500PS spectrometer. Electrospray ionization (ESI) and Tandem mass spectrometry were performed on Bruker ESI timsTOF mass spectrometer. UV/Vis spectra were recorded on a Jasco V-560 spectrophotometer. Corrected emission spectra were obtained by using a Jasco FP-6500 spectrofluorometer. Lifetime measurements were conducted by using a streak camera (Hamamatsu C4334) as a detector and the third-harmonic generation of an Nd:YAG Laser (Continuum Minilite). Emission quantum yields were determined by using a Hamamatsu Photonic Absolute PL Quantum Yield Measurement System C9920-02. Solvents and reagents were used as purchased. Resorcin[4]arene **1a** (R = $C_{11}H_{23}$) and **1b** (R = Me) were prepared according to an established method and purified by recrystallization from acetone/water mixture. The chloride salt of Ir complex $[Ir(ppy)_2(bpy)]Cl$ was synthesized according to the literature. The salts of polyatomic ions $[Ir(ppy)_2(bpy)]X$ (X = NO_2, NO_3, BF_4, ClO_4, PF_6, and OTf) and the other halides $[Ir(ppy)_2(bpy)]X$ (X = Br and I) were obtained by anion exchange reactions using $[Ir(ppy)_2(bpy)]Cl$ with Ag salts in CH_3CN and $[Ir(ppy)_2(bpy)]PF_6$ with potassium salts (KBr and KI) in $CHCl_3$, respectively. All Ir complex salts were purified by recrystallization before using.

General procedure of encapsulation experiments

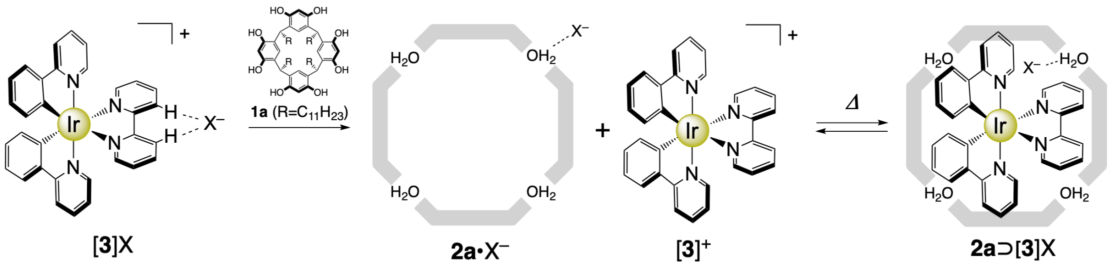

To a wet chloroform solution (0.5 mL) of resorcin[4]arene **1a** (6.6 µmol) was added $[Ir(ppy)_2(bpy)]X$ ([**3**]X, 1.0 µmol). After the mixture was heated at 50 ºC for 1 h in dark, the formation of host–guest complex **2a**⊃[**3**]X was followed by NMR spectroscopy.

^{1}H and DOSY NMR spectra of [3]Br in the presence of 1a

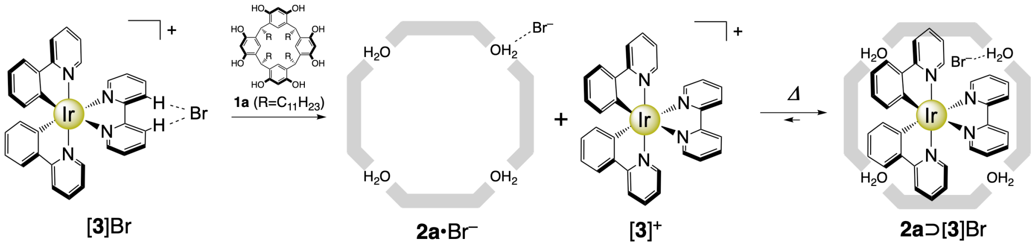

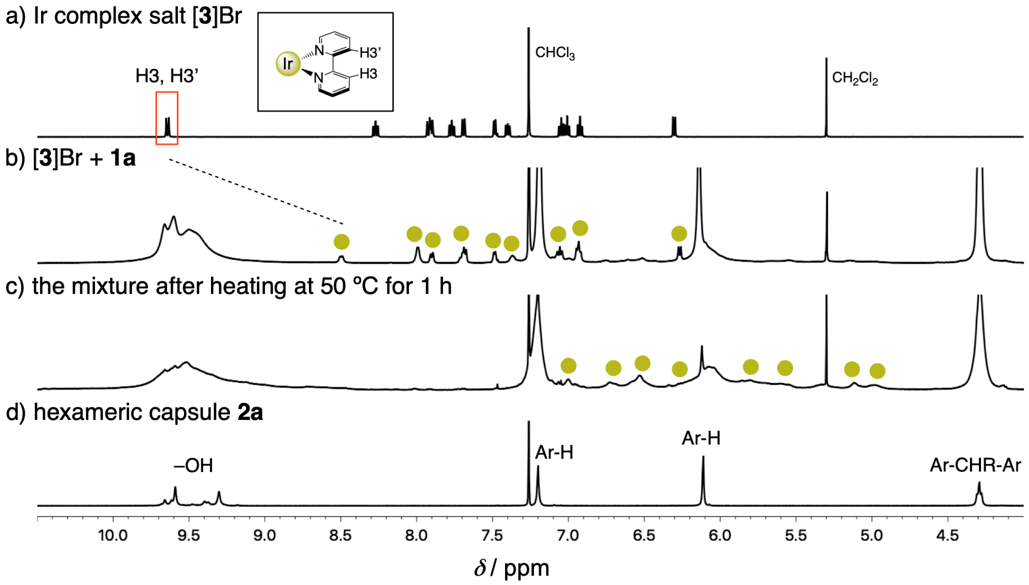

Figure S1. ^{1}H NMR spectra (500 MHz, $CDCl_3$, r.t.) of a) Ir complex salt [**3**]Br, b) the mixture of [**3**]Br and resorcin[4]arene **1a** before heating, c) the mixture after heating at 50 ºC for 1 h, and d) hexameric capsule **2a**. The H3 and H3' protons in the bpy ligand of $[\mathbf{3}]^+$ were considerably shifted to up-field region ($\Delta\lambda = -1.1$ ppm) probably because the Br anion was captured by the capsule. After heating the mixture, no free [**3**]Br was observed, indicating that the ion-pair was stabilized significantly within the capsule.

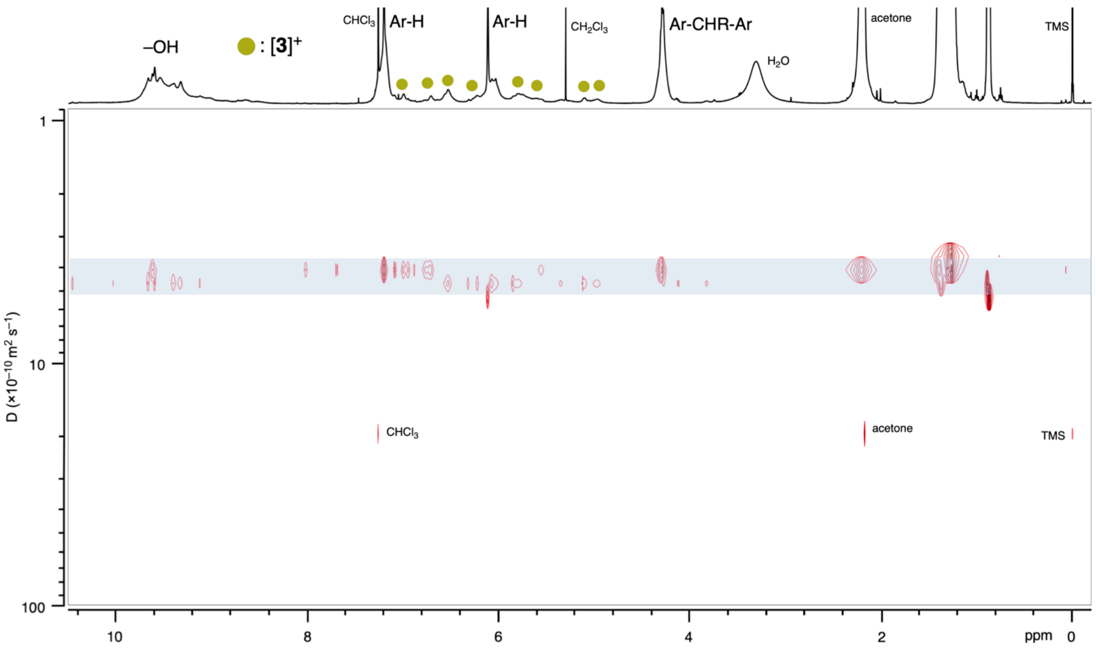

Figure S2. DOSY NMR spectrum (500 MHz, $CDCl_3$, r.t.) of **2a**⊃[**3**]Br.

^{1}H NMR spectra of the guest exchange reaction of 2a⊃[3]Br with [TBA]Br

To a $CDCl_3$ solution containing the encapsulated [Ir(ppy)$_2$(bpy)]Br ([**3**]Br, 1.0 µmol) within resorcin[4]arene **1a** (7.0 µmol) (**2a**⊃[**3**]Br) was added [TBA]Br (3.0 µmol). After the mixture was heated at 50 ºC for 1 h, the guest exchange and the formation of host–guest complex **2a**⊃[TBA]Br were confirmed by ^{1}H NMR spectroscopy.

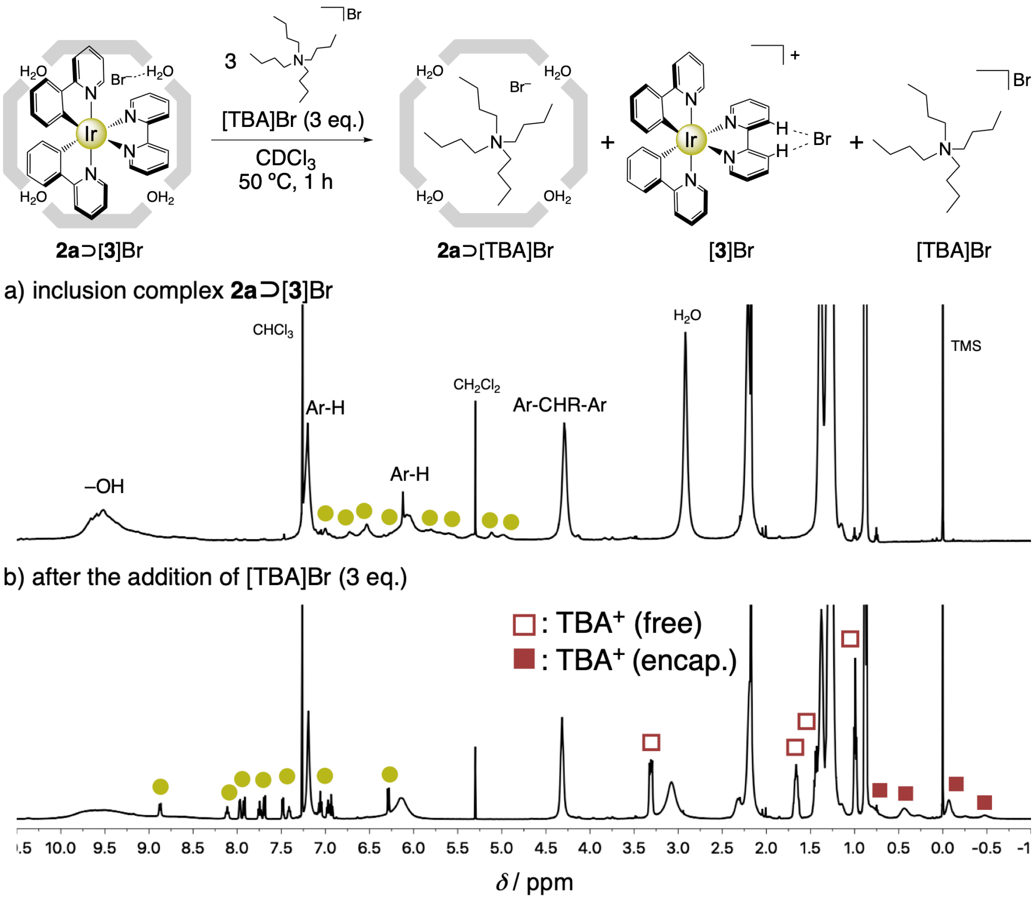

Figure S3. ^{1}H NMR spectra (500 MHz, $CDCl_3$, r.t.) of a) host–guest complex **2a**⊃[**3**]Br and b) the mixture after the addition of 3 equiv. of tetrabutylammonium bromide ([TBA]Br). The addition of TBA salt into a solution of inclusion complex **2a**⊃[**3**]Br afforded a mixture of host–guest complex **2a**⊃[TBA]Br, free Ir complex salt [**3**]Br, and free TBA salt, indicating that guest exchange reaction proceeded to release the Ir complex cation [**3**]$^+$ from the capsule.

^{1}H NMR spectra of [3]NO_2 in the presence of 1a

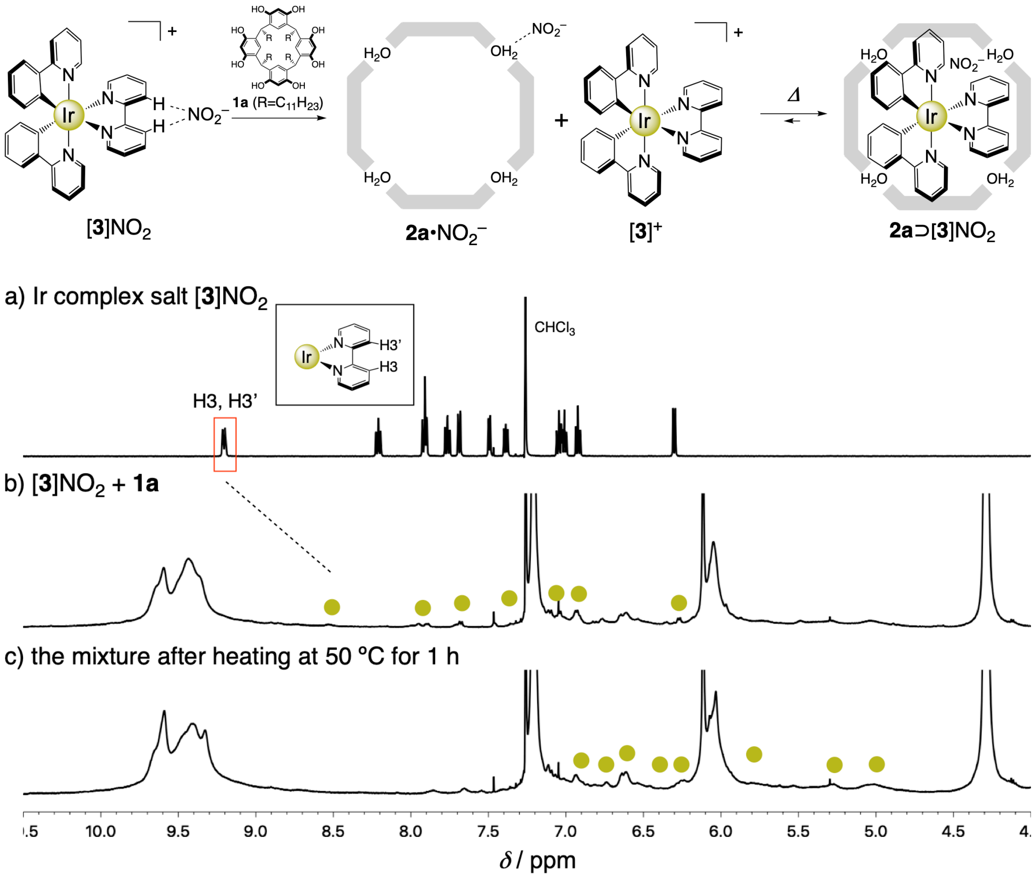

Figure S4. ^{1}H NMR spectra (500 MHz, $CDCl_3$, r.t.) of a) Ir complex salt [**3**]NO_2, b) the mixture of [**3**]NO_2 and resorcin[4]arene **1a** after mixing for 5 min, and c) the mixture after heating at 50 ºC for 1 h. The H3 and H3' protons in the bpy ligand of $[\mathbf{3}]^+$ were considerably shifted to up-field region ($\Delta\lambda = -0.7$ ppm) probably because the NO_2 anion was captured by the capsule. The encapsulation of [**3**]NO_2 proceeded smoothly at room temperature. After heating the mixture, free [**3**]NO_2 was not observed, indicating that the ion-pair was stabilized significantly within the capsule.

^{1}H NMR spectra of [3]I in the presence of 1a

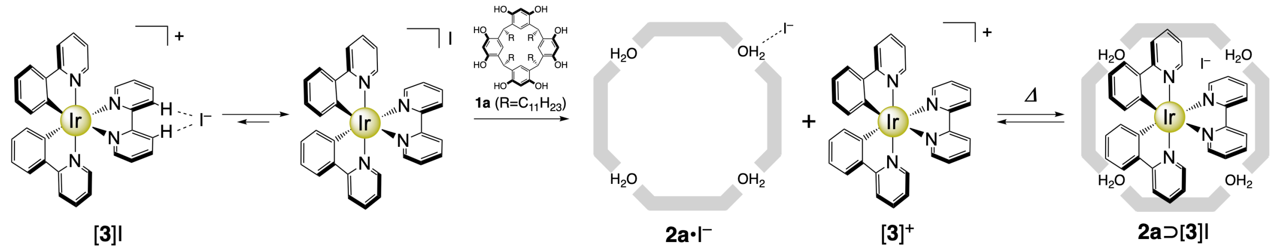

[3]I

1a (R=$C_{11}H_{23}$)

2a•I⁻

[3]⁺

2a⊃**[3]**I

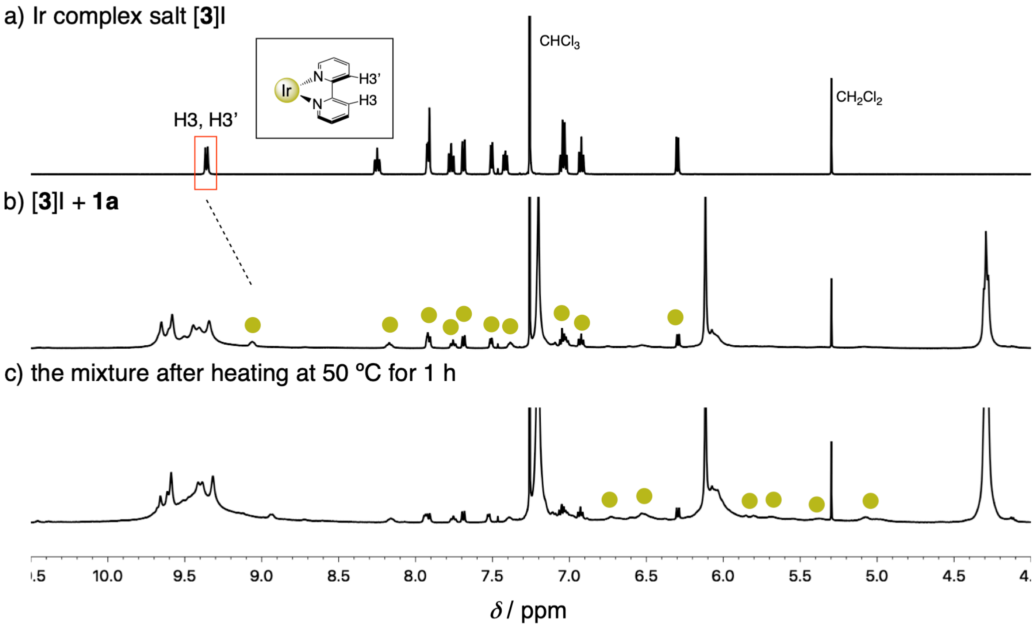

Figure S5. ^{1}H NMR spectra (500 MHz, $CDCl_3$, r.t.) of a) Ir complex salt [**3**]I, b) the mixture of [**3**]I and resorcin[4]arene **1a** before heating, and c) the mixture after heating at 50 ºC for 1 h. The H3 and H3’ protons in the bpy ligand of $[3]^+$ were slightly shifted to up-field region ($\Delta\lambda$ = –0.3 ppm) probably because of the weak hydrogen-bonding ability of iodide ion. After heating the mixture, both free and encapsulated $[3]^+$ were observed. These results indicate that the ion-pair is not stabilized enough because of the size of the ion-pair comparable to the capacity of the cavity.

^{1}H NMR spectra of [3]NO$_3$ in the presence of 1a

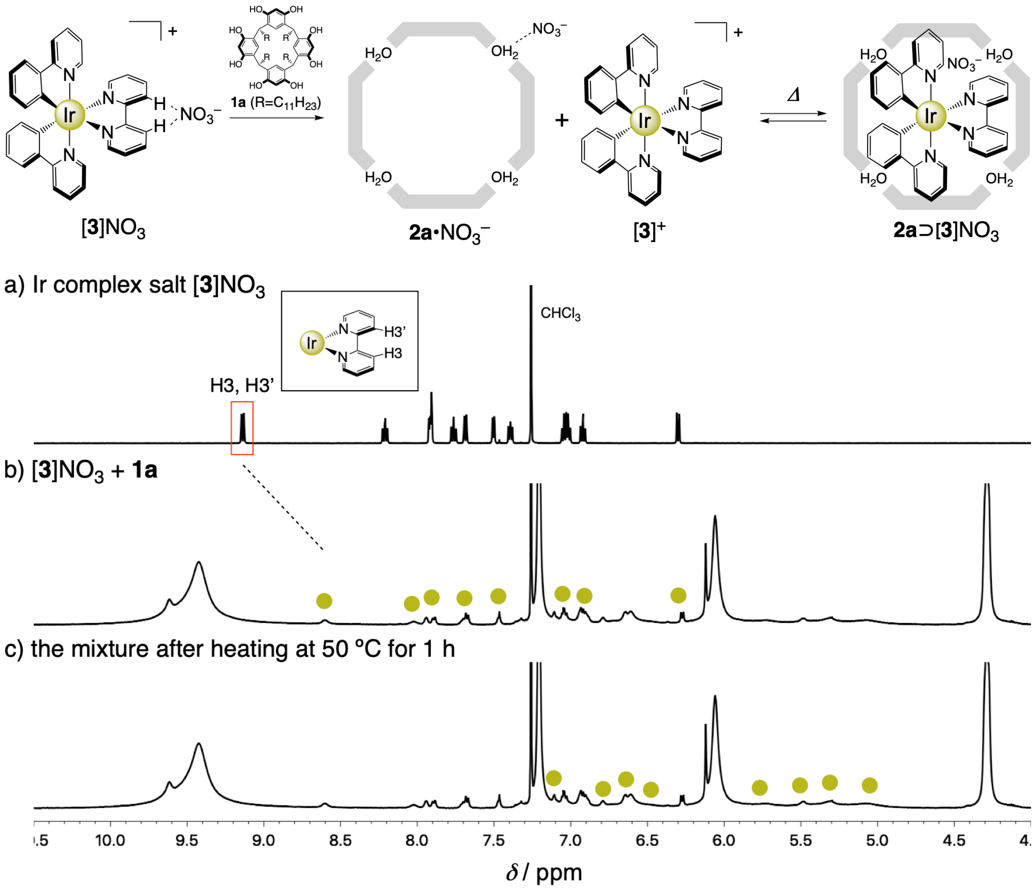

Figure S6. ^{1}H NMR spectra (500 MHz, $CDCl_3$, r.t.) of a) Ir complex salt [**3**]NO_3, b) the mixture of [**3**]NO_3 and resorcin[4]arene **1a** before heating, and c) the mixture after heating at 50 ºC for 1 h. The H3 and H3' protons in the bpy ligand of [**3**]$^+$ were slightly shifted to up-field region ($\Delta\lambda = -0.6$ ppm) probably NO_3 anion was captured by the capsule. The encapsulation of [**3**]NO_3 proceeded smoothly at room temperature. After heating the mixture, both free and encapsulated [**3**]$^+$ were observed. These results indicate that the ion-pair is not stabilized enough because of the size of the ion-pair comparable to the capacity of the cavity.

^{1}H and ^{19}F NMR spectra of [3]BF$_4$ in the presence of 1a

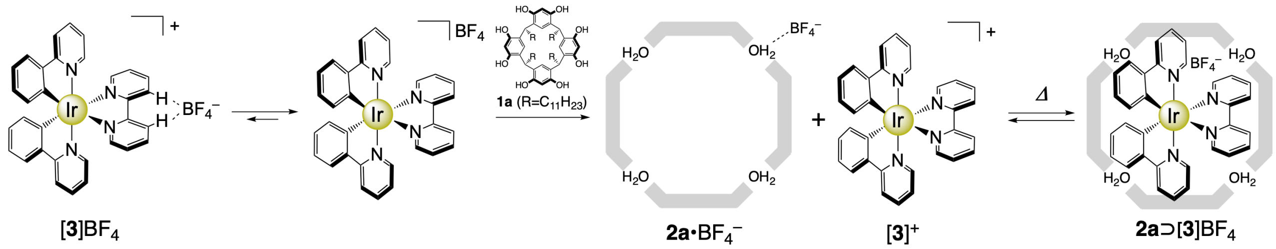

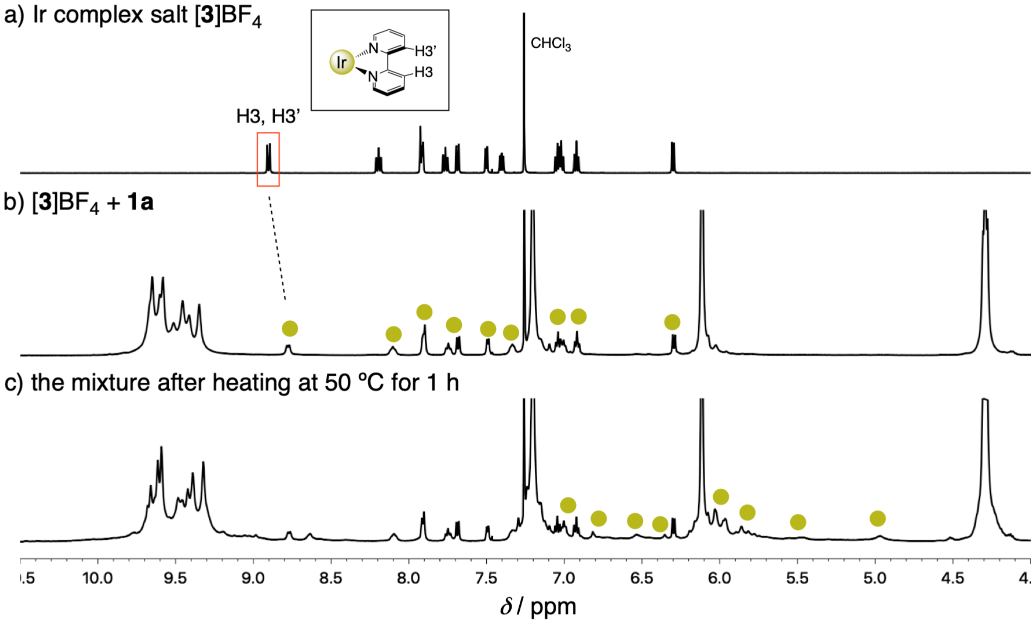
a) Ir complex salt [3]BF$_4$

b) [3]BF$_4$ + 1a

c) the mixture after heating at 50 °C for 1 h

Figure S7. ^{1}H NMR spectra (500 MHz, $CDCl_3$, r.t.) of a) Ir complex salt [**3**]BF$_4$, b) the mixture of [**3**]BF$_4$ and resorcin[4]arene **1a** before heating, and c) the mixture after heating at 50 ºC for 1 h. The H3 and H3' protons in the bpy ligand of [3]$^+$ were slightly shifted to up-field region ($\Delta\lambda = -0.2$ ppm) probably because of the weak hydrogen-bonding ability of BF_4^- ion. After heating the mixture, both free and encapsulated [3]$^+$ were observed. These results indicate that the ion-pair is not stabilized enough because of the size of the ion-pair comparable to the capacity of the cavity.

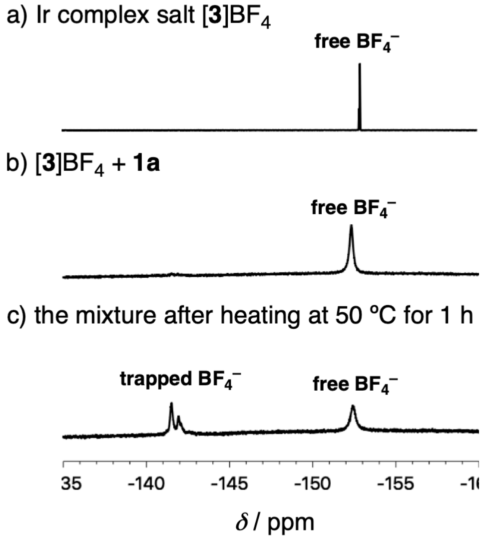
a) Ir complex salt [3]BF$_4$

b) [3]BF$_4$ + 1a

c) the mixture after heating at 50 °C for 1 h

Figure S8. ^{19}F NMR spectra (470 MHz, $CDCl_3$, r.t.) of a) Ir complex salt [**3**]BF$_4$, b) the mixture of [**3**]BF$_4$ and resorcin[4]arene **1a** before heating, and c) the mixture after heating at 50 ºC for 1 h. New peak at –142 ppm appeared after heating the sample, which can be assigned to trapped BF$_4$ anion within the capsule.

^{1}H NMR spectra of [3]ClO_4 in the presence of 1a

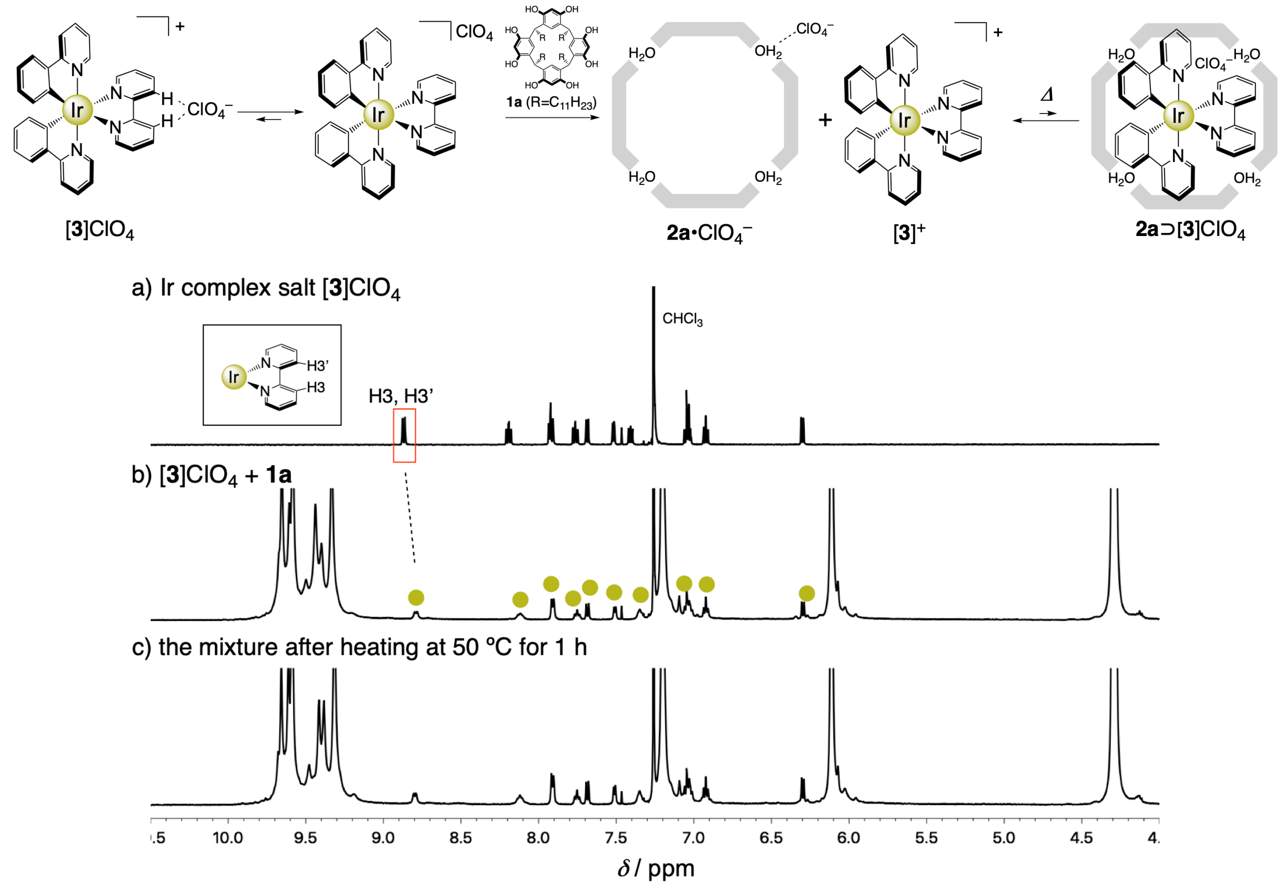

Figure S9. ^{1}H NMR spectra (500 MHz, $CDCl_3$, r.t.) of a) Ir complex salt [**3**]ClO_4, b) the mixture of [**3**]ClO_4 and resorcin[4]arene **1a** before heating, and c) the mixture after heating at 50 ºC for 1 h. The H3 and H3' protons in the bpy ligand of $[3]^+$ were slightly shifted to up-field region ($\Delta\lambda = -0.1$ ppm) probably because of the weak hydrogen-bonding ability of ClO_4^- ion. After heating the mixture, free [**3**]$^+$ was predominantly observed. These results indicate that the formation of the ion-pair is thermodynamically disfavored within the capsule.

^{1}H and ^{19}F NMR spectra of [3]PF$_6$ in the presence of 1a

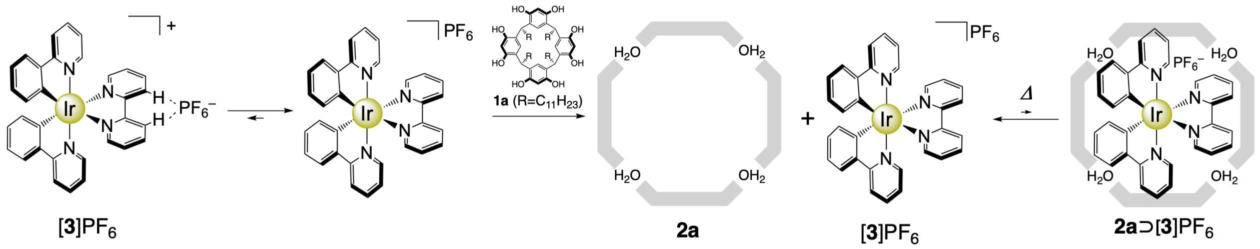

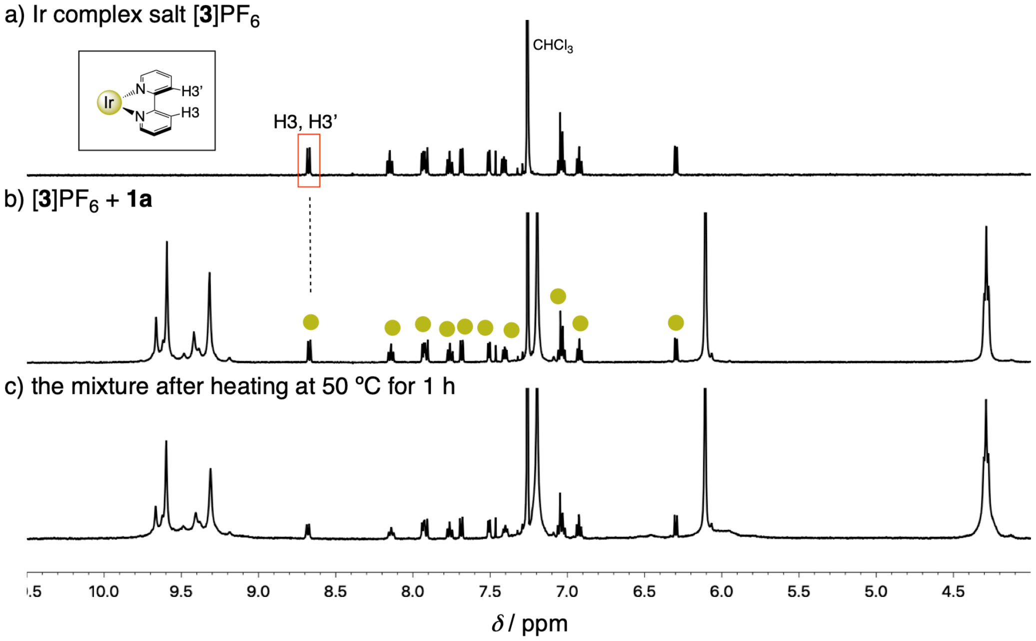

Figure S10. ^{1}H NMR spectra (500 MHz, $CDCl_3$, r.t.) of a) Ir complex salt [**3**]PF$_6$, b) the mixture of [**3**]PF$_6$ and resorcin[4]arene **1a** before heating, and c) the mixture after heating at 50 ºC for 1 h. The H3 and H3' protons in the bpy ligand of [**3**]$^+$ were not shifted probably because of the negligible hydrogen-bonding ability of PF_6^- ion. After heating the mixture, only free [**3**]$^+$ was observed. These results indicate that the ion-pair is not stabilized enough for PF_6 anion because the size of the ion-pair is larger than the capacity of the cavity.

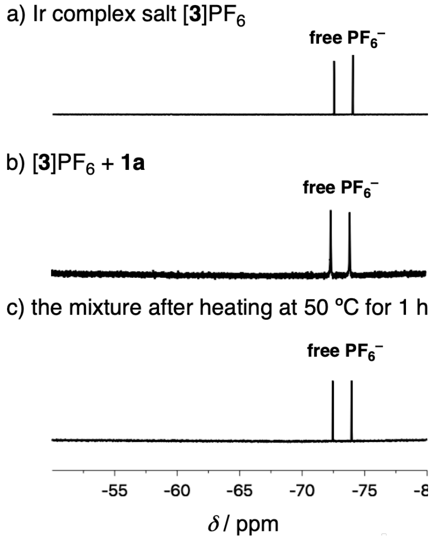

Figure S11. ^{19}F NMR spectra (470 MHz, $CDCl_3$, r.t.) of a) Ir complex salt [**3**]PF$_6$, b) the mixture of [**3**]PF$_6$ and resorcin[4]arene **1a** before heating, and c) the mixture after heating at 50 ºC for 1 h. No new peak was observed after heating the sample, suggesting that the PF_6 anion was not trapped within the capsule.

^{1}H and ^{19}F NMR spectra of [3]OTf in the presence of 1a

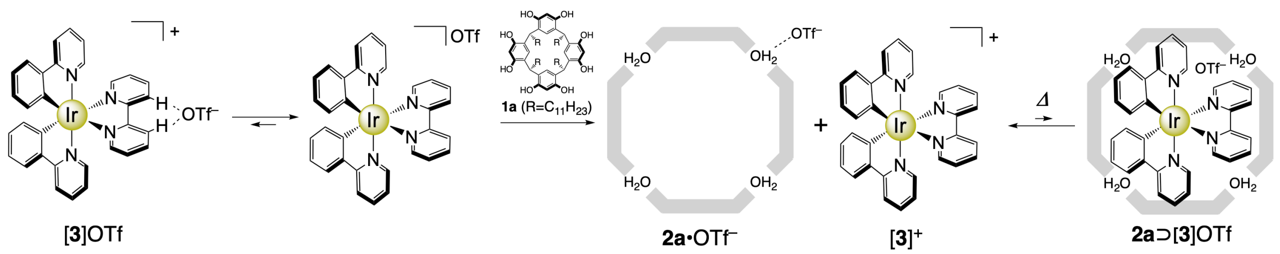

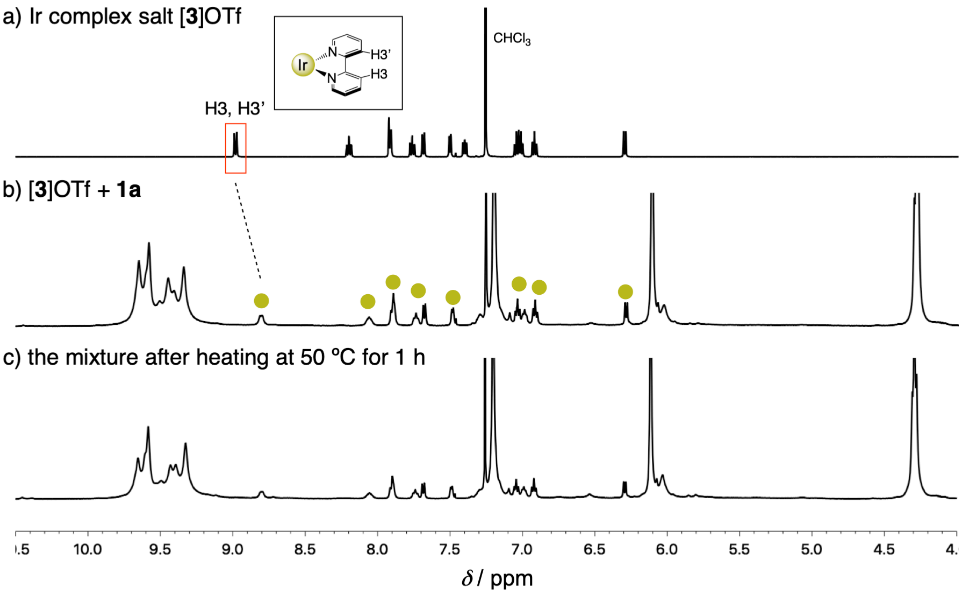

Figure S12. ^{1}H NMR spectra (500 MHz, CDCl$_3$, r.t.) of a) Ir complex salt [**3**]OTf, b) the mixture of [**3**]OTf and resorcin[4]arene **1a** before heating, and c) the mixture after heating at 50 °C for 1 h. The H3 and H3' protons in the bpy ligand of [3]$^+$ were slightly shifted to up-field region ($\Delta\lambda$ = –0.2 ppm) probably because of the weak hydrogen-bonding ability of OTf$^-$ ion. After heating the mixture, free [**3**]$^+$ was predominantly observed. These results indicate that the formation of the ion-pair is thermodynamically disfavored within the capsule.

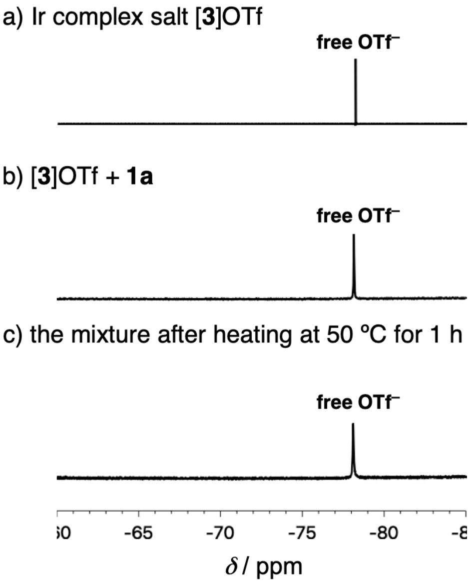

Figure S13. ^{19}F NMR spectra (470 MHz, CDCl$_3$, r.t.) of a) Ir complex salt [**3**]OTf, b) the mixture of [**3**]OTf and resorcin[4]arene **1a** before heating, and c) the mixture after heating at 50 °C for 1 h. No new peak was observed after heating the sample, suggesting that the OTf anion was not trapped within the capsule.

^{1}H NMR spectra of [3]X (X = Cl, Br, I, NO$_2$, NO$_3$, OTf, BF$_4$, ClO$_4$, and PF$_6$)

The counter anion-dependent down-field shifts of H3 and H3' protons on the bpy ligand in [**3**]$^+$ indicate that the extent of down-field shifts is correlated with the hydrogen-bonding abilities of counter anions. It is noted that monoatomic anions (X = Cl$^-$, Br$^-$, and I$^-$) showed larger down-field shifts, compared to polyatomic anions, probably because of smaller entropy loss upon the formation of chelating form [**3**]X.

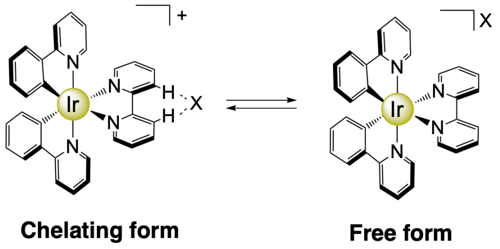

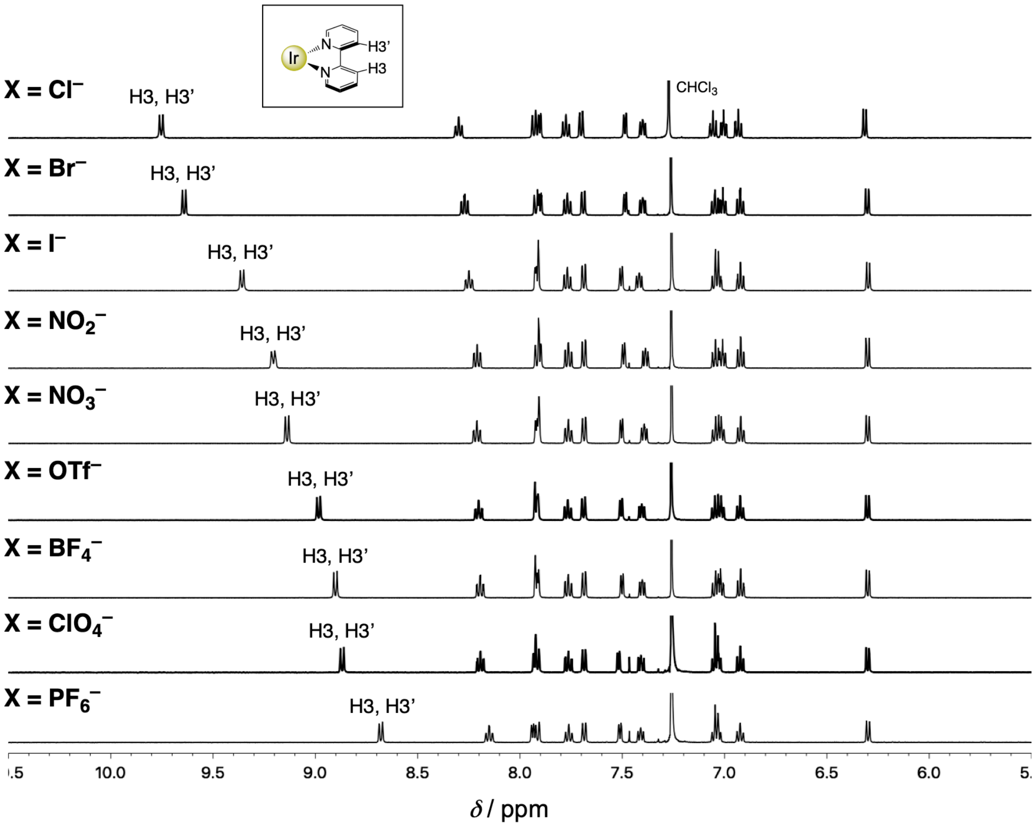

Figure S14. ^{1}H NMR spectra (500 MHz, CDCl$_3$, r.t.) of Ir complex salts [**3**]X.

Table S1. Chemical shifts of H3 and H3' protons of the Ir complex salts.

Counter Anion	Chemical shift (ppm)	H-bond acceptor parameters (β)[a]	Counter Anion	Chemical shift (ppm)	H-bond acceptor parameters (β)[a]
Cl$^-$	9.75	12.1 ± 0.3	NO$_2^-$	9.20	–
Br$^-$	9.65	10.6 ± 0.2	NO$_3^-$	9.14	10.7 ± 0.5
I$^-$	9.36	9.1 ± 0.1	OTf$^-$	8.98	9.4 ± 0.4
			BF$_4^-$	8.90	–
			ClO$_4^-$	8.87	8.3 ± 0.4
			PF$_6^-$	8.68	7.0 ± 0.3

[a] ref. 19 in the main text.

ESI-MS and MS-MS spectra of [3]$^+$ in the presence of resorcin[4]arene 1b (R = Me)

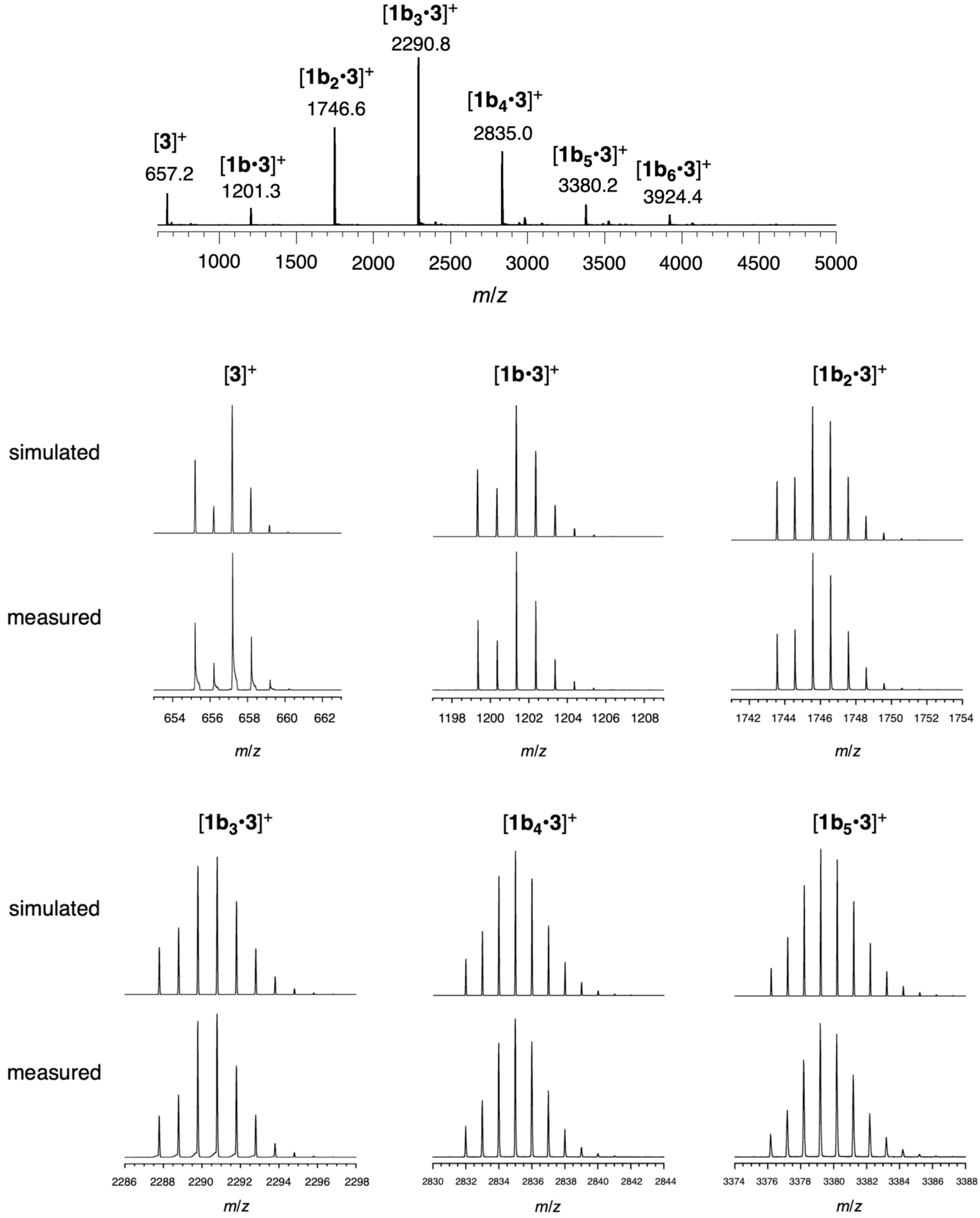

Figure S15. ESI-MS spectra of a mixture of Ir complex salt and resorcin[4]arene **1b** (R = Me) in CHCl$_3$/acetone (2:1). The template effect of the complex cation effectively stabilizes self-assembly of hydrogen-bonded resorcin[4]arene capsules even in a gas phase. Fragmentation of [**1b$_6$•3**]$^+$ under the measurement condition afford host–guest complex [**1b$_3$•3**]$^+$ as the most intense peak.

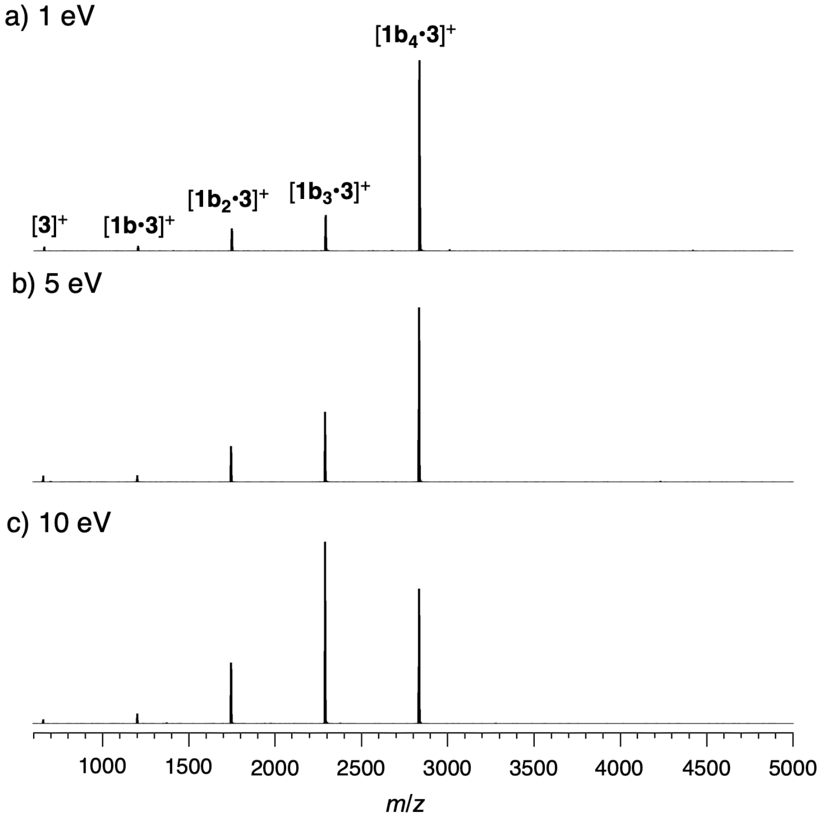

Figure S16. ESI tandem mass spectrum of [**1b**$_4$•**3**]$^+$ (m/z : 2835) with the collision energy at a) 1 eV, b) 5 eV, and c) 10 eV. Higher collision energy promotes consecutive monomer losses from the parent ion.

Photophysical data of [3]X (X = Cl, Br, NO_2, I, NO_3, BF_4, ClO_4, PF_6, and OTf)

All measurements were performed in 10 μM $CHCl_3$ solution of the analytes in the absence and presence of various amount of resorcin[4]arene **1a** at room temperature under degassed conditions through N_2 bubbling for 30 min. In the latter case (in the presence of **1a**), the sample solutions were heated at 50 °C for 5 min and cooled to room temperature prior to photophysical measurement. Emission decay curves of the Ir complex salts and the host–guest complexes were analysed by a single exponential decay ($I(t) = A_1\exp(-t/\tau)$) and a bi-exponential decay ($I(t) = A_1\exp(-t/\tau_1) + A_2\exp(-t/\tau_2)$) using the nonlinear least-squares method, respectively. The averaged emission lifetime (τ_{ave}) was estimated by the equation ($\tau_{ave} = A_1\tau_1^2 + A_2\tau_2^2 / A_1\tau_1 + A_2\tau_2$). The radiative rate constants (k_r) and nonradiative rate constants (k_{nr}) were estimated using an equation: $\Phi = k_r / (k_r + k_{nr}) = k_r\tau$.

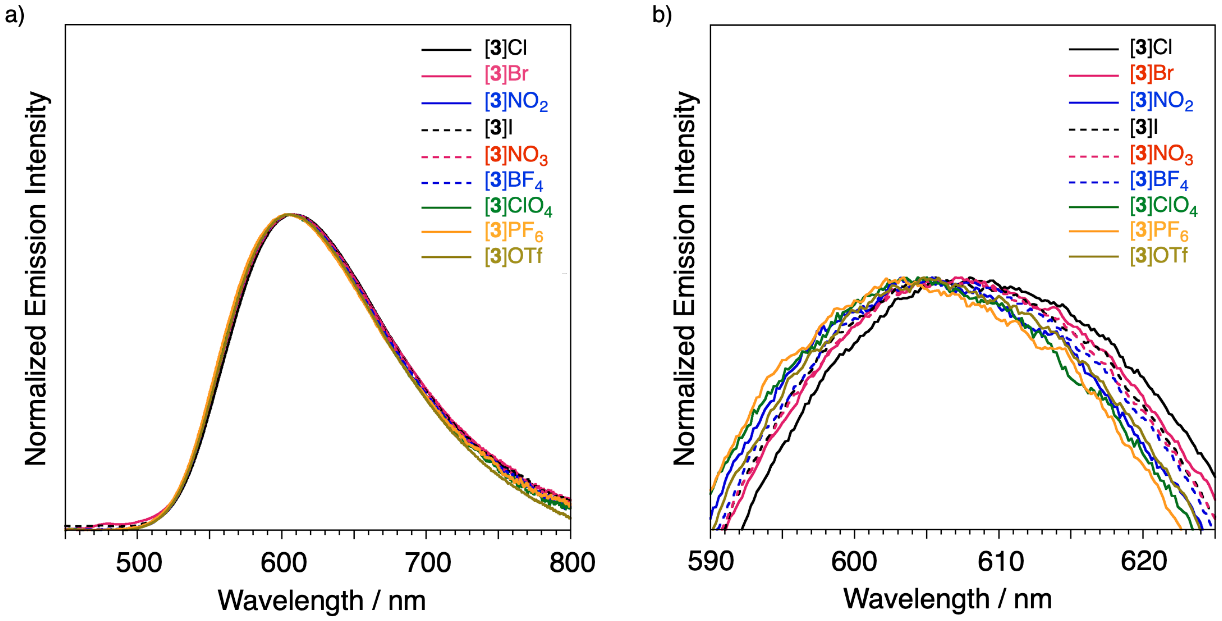

Figure S17. a) Normalized emission spectra (10 μM, $CHCl_3$, r.t.) of the Ir complex salts and b) enlarged spectra around the peak top (λ_{ex} = 400 nm). All emission spectra almost overlap, indicating that the emission wavelength of the Ir complex cation was independent on their counter anions.

Table S2. Photophysical data (10 μM, $CHCl_3$, r.t.) of [**3**]X (X = Cl, Br, NO_2, I, NO_3, BF_4, ClO_4, PF_6, and OTf).

Complex	λ_{em} [nm]	Φ [%][a]	τ [ns][b]	k_r [$\times 10^5$ s^{-1}]	k_{nr} [$\times 10^6$ s^{-1}]
[**3**]Cl	609	20	420	4.8	1.9
[**3**]Br	608	23	430	5.3	1.8
[**3**]NO_2	607	15	360	4.5	2.1
[**3**]I	605	14	360	3.9	2.4
[**3**]NO_3	606	22	360	6.1	2.2
[**3**]BF_4	605	23	440	5.3	1.8
[**3**]ClO_4	605	26	400	6.5	1.9
[**3**]PF_6	604	26	410	6.3	1.8
[**3**]OTf	604	20	440	4.5	1.8

[a] All measurements were performed in $CHCl_3$ at room temperature under degassed conditions. [b] analysed by a single exponential decay.

Photophysical data of [3]Br in the presence of 1a

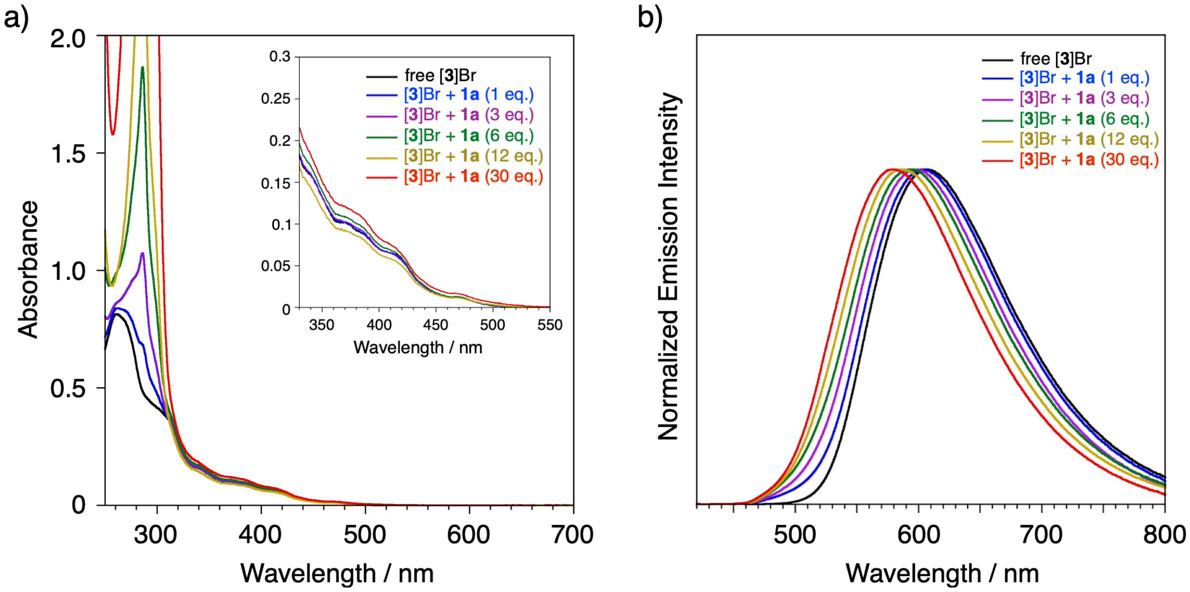

Figure S18. a) UV-vis absorption and b) normalized emission spectra of the [**3**]Br (10 μM , $CHCl_3$, r.t.) in the presence of **1a** (λ_{ex} = 400 nm). The absorption spectra of $[\mathbf{3}]^+$ did not change significantly after encapsulation, meanwhile the emission spectra of $[\mathbf{3}]^+$ showed blue-shift upon addition of **1a**.

Table S3. Photophysical data (10 μM for [**3**]Br, $CHCl_3$, r.t.) with various amounts of **1a**.

[**1a**] [μM]	λ_{em} [nm]	Φ [%]	A_1	τ_1 [ns]	A_2	τ_2 [ns]	τ_{ave} [ns]	k_r [× 10^5 s^{-1}]	k_{nr} [× 10^6 s^{-1}]
0	608	23	0.20	430[a]				5.3	1.8
10	603	23	0.79	350	0.21	1030	650	3.5	1.2
30	599	25	0.70	470	0.30	1160	820	3.0	0.91
60	593	28	0.63	500	0.37	1140	870	3.2	0.83
120	585	32	0.62	670	0.38	1240	970	3.2	0.70
300	580	34	0.59	650	0.41	1220	970	3.5	0.68

[a] analysed by a single exponential decay.

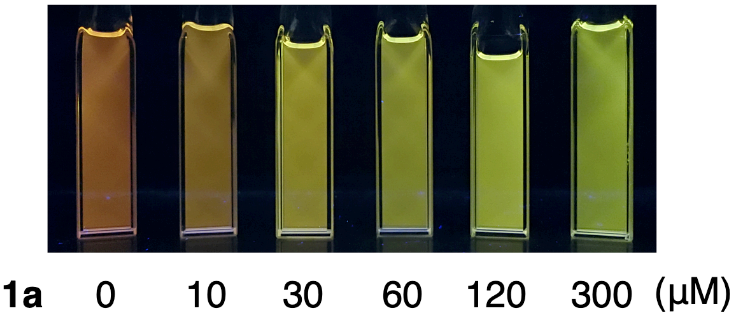

Figure S19. Photographic images of the $CHCl_3$ solutions (10 μM for [**3**]Br) with various amounts of **1a** under photoirradiation (λ_{ex} = 365 nm).

Photophysical data of [3]NO₂ in the presence of 1a

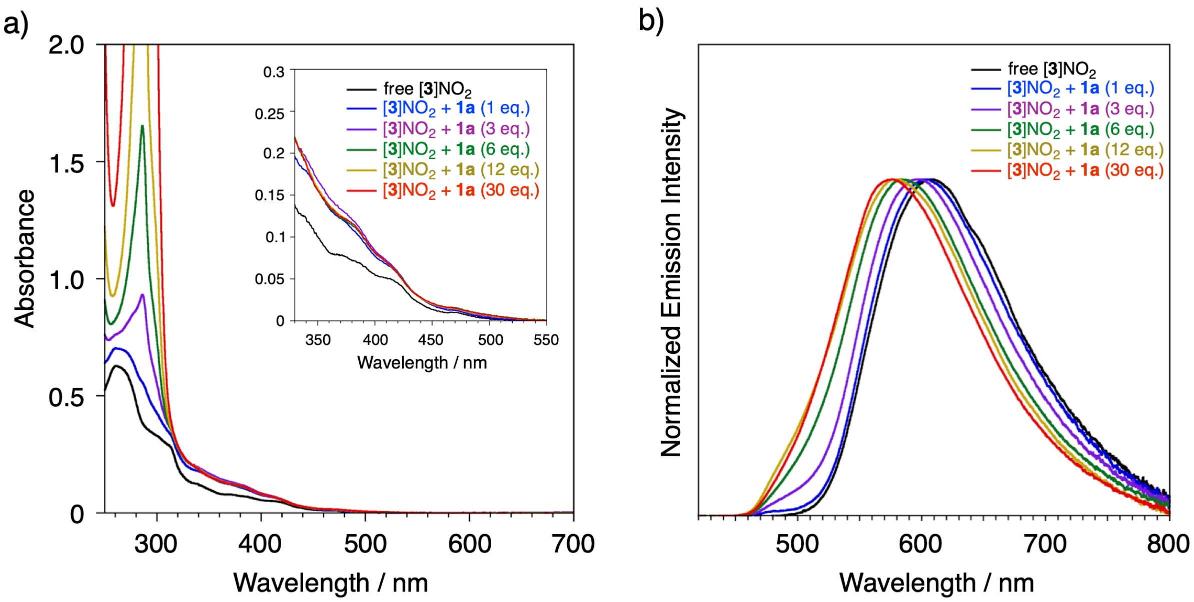

Figure S20. a) UV-vis absorption and b) normalized emission spectra of the [**3**]NO$_2$ (10 µM, CHCl$_3$, r.t.) in the presence of **1a** (λ_{ex} = 400 nm). The absorption spectra of [**3**]$^+$ did not change significantly after encapsulation, meanwhile the emission spectra of [**3**]$^+$ showed blue-shift upon addition of **1a**.

Table S4. Photophysical data (10 µM for [**3**]NO$_2$, CHCl$_3$, r.t.) with various amounts of **1a**.

[**1a**] [µM]	λ_{em} [nm]	Φ [%]	A$_1$	τ_1 [ns]	A$_2$	τ_2 [ns]	τ_{ave} [ns]	k_r [× 10^5 s^{-1}]	k_{nr} [× 10^6 s^{-1}]
0	607	15	0.18	360[a]				4.5	2.1
10	604	10	0.85	390	0.15	870	520	1.9	1.7
30	596	12	0.72	400	0.28	890	630	1.9	1.4
60	583	13	0.54	330	0.60	960	780	1.7	1.1
120	577	13	0.36	450	0.64	1030	910	1.4	0.95
300	576	13	0.38	510	0.62	1070	940	1.4	0.92

[a] analysed by a single exponential decay.

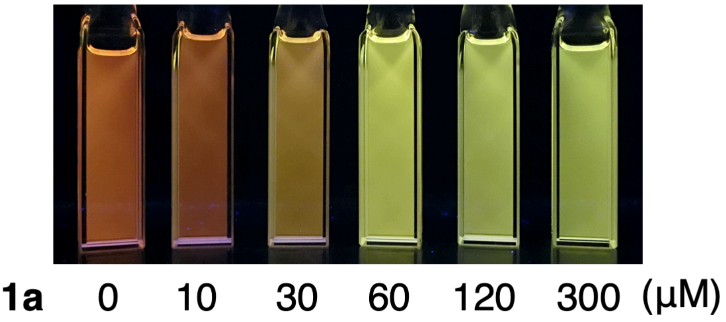

Figure S21. Photographic images of the CHCl$_3$ solutions (10 µM for [**3**]NO$_2$) with various amounts of **1a** under photoirradiation (λ_{ex} = 365 nm).

Photophysical data of [3]I in the presence of 1a

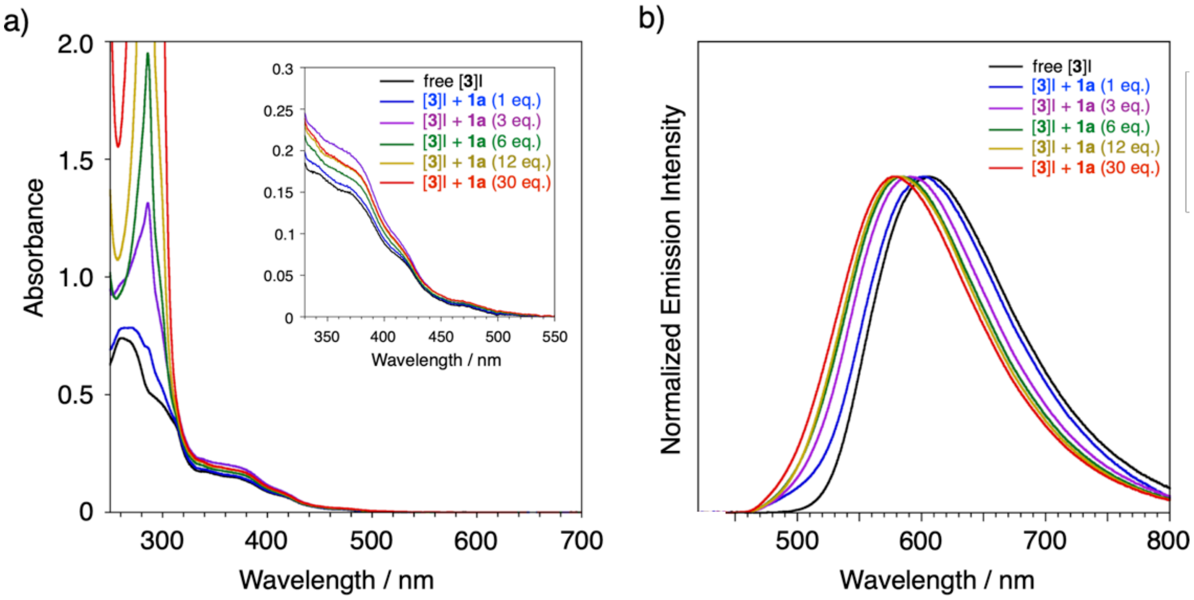

Figure S22. a) UV-vis absorption and b) normalized emission spectra of the [**3**]I (10 µM, $CHCl_3$, r.t.) in the presence of **1a** (λ_{ex} = 400 nm). The absorption spectra of $[\mathbf{3}]^+$ did not change significantly after encapsulation, meanwhile the emission spectra of $[\mathbf{3}]^+$ showed blue-shift upon addition of **1a**.

Table S5. Photophysical data (10 µM for [**3**]I, $CHCl_3$, r.t.) with various amounts of **1a**.

[**1a**] [µM]	λ_{em} [nm]	Φ [%]	A_1	τ_1 [ns]	A_2	τ_2 [ns]	τ_{ave} [ns]	k_r [$\times 10^5$ s^{-1}]	k_{nr} [$\times 10^6$ s^{-1}]
0	605	14	0.18	360[a]				3.9	2.4
10	602	14	0.80	380	0.20	1110	690	2.0	1.2
30	591	15	0.67	490	0.33	1150	850	1.8	1.0
60	584	18	0.55	540	0.45	1090	880	2.0	0.93
120	581	18	0.59	630	0.41	1170	930	1.9	0.88
300	579	19	0.56	680	0.44	1230	1000	1.9	0.81

[a] analysed by a single exponential decay.

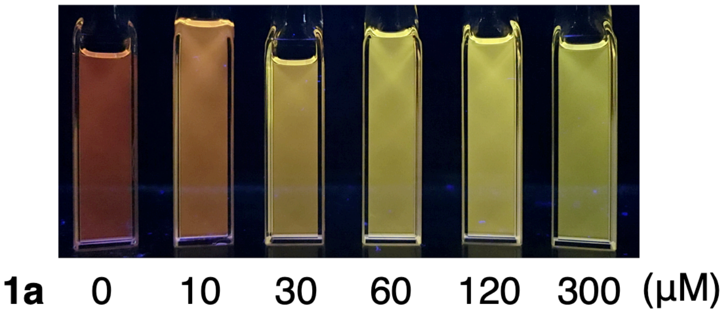

Figure S23. Photographic images of the $CHCl_3$ solutions (10 µM for [**3**]I) with various amounts of **1a** under photoirradiation (λ_{ex} = 365 nm).

Photophysical data of [3]NO$_3$ in the presence of 1a

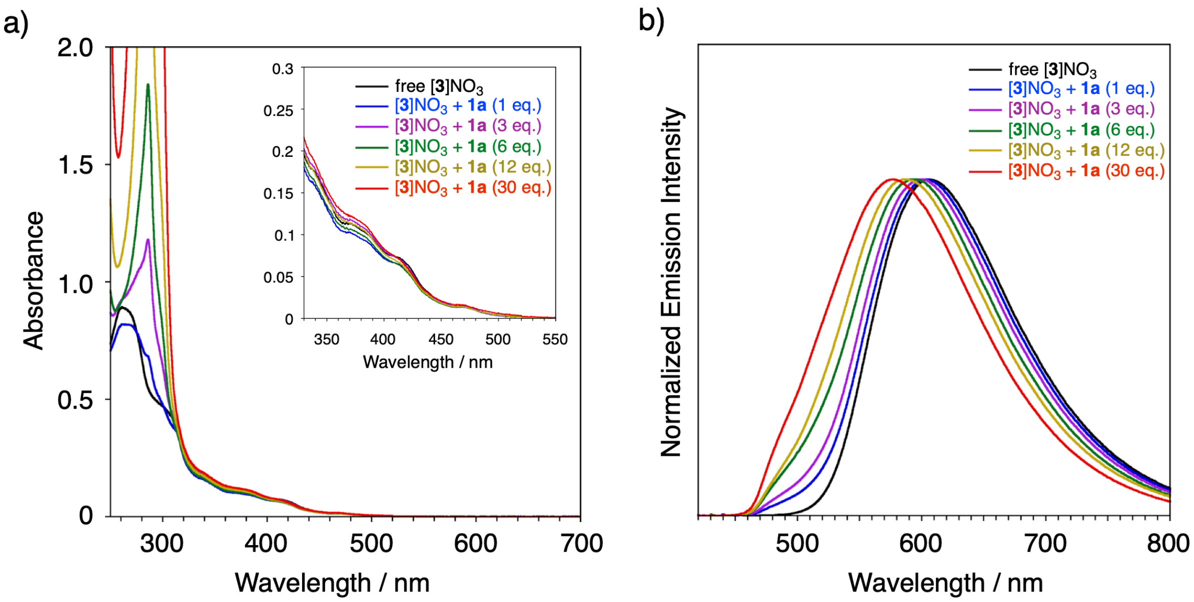

Figure S24. a) UV-vis absorption and b) normalized emission spectra-of the [**3**]NO$_3$ (10 μM, CHCl$_3$, r.t.) in the presence of **1a** (λ_{ex} = 400 nm). The absorption spectra of [**3**]$^+$ did not change significantly after encapsulation, meanwhile the emission spectra of [**3**]$^+$ showed blue-shift upon addition of **1a**.

Table S6. Photophysical data of [3]NO$_3$ in the presence of **1a**.

[**1a**] [μM]	λ_{em} [nm]	Φ [%]	A_1	τ_1 [ns]	A_2	τ_2 [ns]	τ_{ave} [ns]	k_r [× 10^5 s^{-1}]	k_{nr} [× 10^6 s^{-1}]
0	606	22	0.20	360[a]				6.1	2.2
10	603	22	0.82	310	0.18	960	570	3.8	1.4
30	599	22	0.66	340	0.34	980	720	3.0	1.1
60	596	23	0.55	420	0.45	1040	840	2.7	0.92
120	586	24	0.46	400	0.54	1050	890	2.6	0.85
300	578	24	0.50	650	0.50	1170	980	2.4	0.77

[*a*] analysed by a single exponential decay.

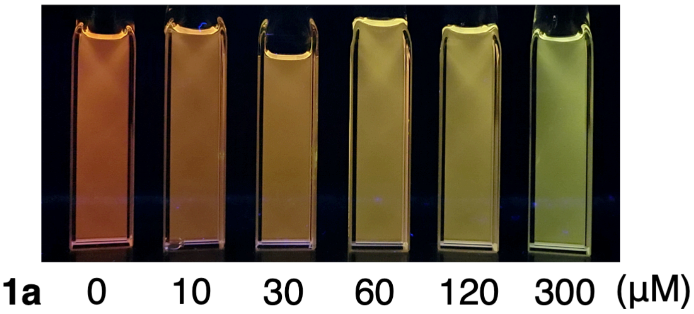

Figure S25. Photographic images of the CHCl$_3$ solutions (10 μM for [**3**]NO$_3$) with various amounts of **1a** under photoirradiation (λ_{ex} = 365 nm).

Photophysical data of [3]BF$_4$ in the presence of 1a

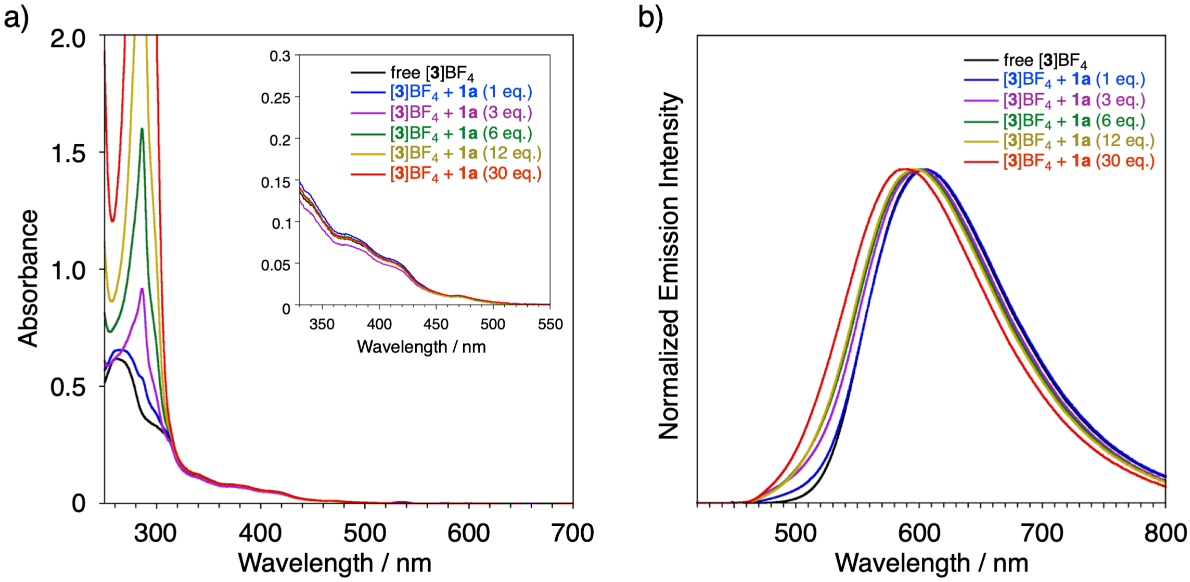

Figure S26. UV-vis absorption and b) normalized emission spectra of the [**3**]BF$_4$ (10 μM, CHCl$_3$, r.t.) in the presence of **1a** (λ_{ex} = 400 nm). The absorption spectra of [**3**]$^+$ did not change significantly after encapsulation, meanwhile the emission spectra of [**3**]$^+$ showed blue-shift upon addition of **1a**.

Table S7. Photophysical data (10 μM for [**3**]BF$_4$, CHCl$_3$, r.t.) with various amounts of **1a**.

[**1a**] [μM]	λ_{em} [nm]	Φ [%]	A_1	τ_1 [ns]	A_2	τ_2 [ns]	τ_{ave} [ns]	k_r [$\times 10^5$ s^{-1}]	k_{nr} [$\times 10^6$ s^{-1}]
0	605	23	0.23	440[a]				5.3	1.8
10	605	23	0.90	370	0.10	970	510	4.5	1.5
30	602	23	0.73	340	0.27	1050	730	3.2	1.1
60	598	27	0.74	470	0.26	1090	750	3.6	0.97
120	596	29	0.06	460	0.40	1020	790	3.6	0.90
300	591	32	0.06	570	0.40	1120	880	3.6	0.77

[*a*] analysed by a single exponential decay.

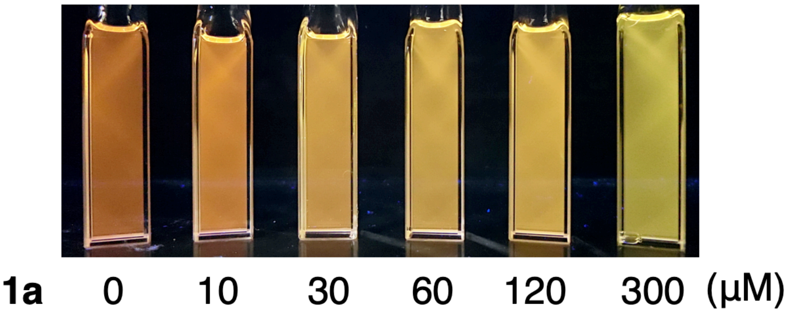

Figure S27. Photographic images of the CHCl$_3$ solutions (10 μM for [**3**]BF$_4$) with various amounts of **1a** under photoirradiation (λ_{ex} = 365 nm).

Photophysical data of [3]ClO$_4$ in the presence of 1a

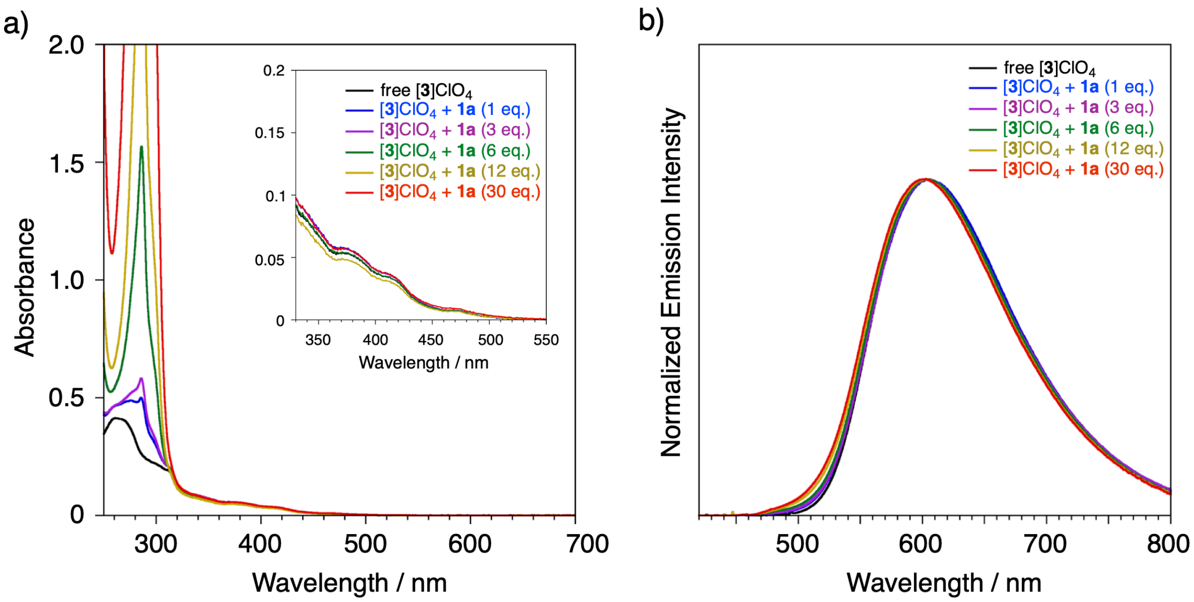

Figure S28. a) UV-vis absorption and b) normalized emission spectra of the [**3**]ClO$_4$ (10 μM, CHCl$_3$, r.t.) in the presence of **1a** (λ_{ex} = 400 nm). The absorption spectra of [**3**]$^+$ did not change significantly after addition of **1a**, and the emission spectra of [**3**]$^+$ showed very small blue-shift.

Table S8. Photophysical data (10 μM for [**3**]ClO$_4$, CHCl$_3$, r.t.) with various amounts of **1a**.

[**1a**] [μM]	λ_{em} [nm]	Φ [%]	A$_1$	τ_1 [ns]	A$_2$	τ_2 [ns]	τ_{ave} [ns]	k_r [× 10^5 s^{-1}]	k_{nr} [× 10^6 s^{-1}]
0	605	26	0.17	400[a]				6.5	1.9
10	605	26	0.94	330	0.06	1150	480	5.4	1.5
30	604	26	0.95	420	0.05	1350	560	4.7	1.3
60	603	26	0.90	410	0.10	1260	630	4.1	1.2
120	602	27	0.85	470	0.15	1230	710	3.8	1.0
300	601	28	0.83	490	0.17	1300	780	3.6	0.92

[*a*] analysed by a single exponential decay.

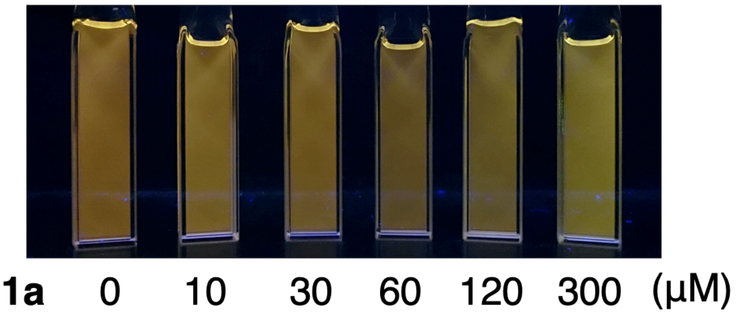

Figure S29. Photographic images of the CHCl$_3$ solutions (10 μM for [**3**]ClO$_4$) with various amounts of **1a** under photoirradiation (λ_{ex} = 365 nm).

Photophysical data of [3]PF$_6$ in the presence of 1a

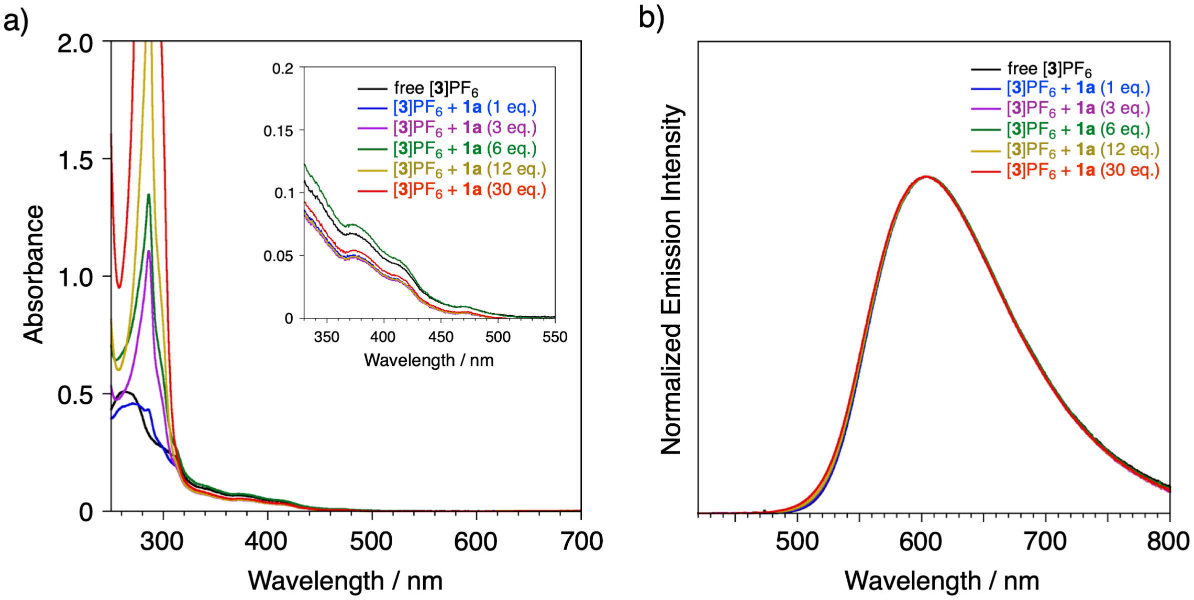

Figure S30. a) UV-vis absorption and b) normalized emission spectra of the [**3**]PF$_6$ (10 µM, CHCl$_3$, r.t.) in the presence of **1a** (λ_{ex} = 400 nm). Both the absorption and emission spectra of [**3**]$^+$ did not change significantly upon addition of **1a**.

Table S9. Photophysical data (10 µM for [**3**]PF$_6$, CHCl$_3$, r.t.) with various amounts of **1a**.

[**1a**] [µM]	λ_{em} [nm]	Φ [%]	A$_1$	τ_1 [ns]	A$_2$	τ_2 [ns]	τ_{ave} [ns]	k_r [× 10^5 s^{-1}]	k_{nr} [× 10^6 s^{-1}]
0	604	26	0.22	410[a]				6.3	1.8
10	604	26	0.98	370	0.98	1210	420	6.2	1.8
30	604	26	0.90	420	0.90	1160	590	4.4	1.2
60	604	26	0.92	460	0.92	1180	590	4.4	1.2
120	603	27	0.89	450	0.89	1170	620	4.4	1.2
300	603	27	0.89	440	0.89	1170	620	4.4	1.2

[*a*] analysed by a single exponential decay.

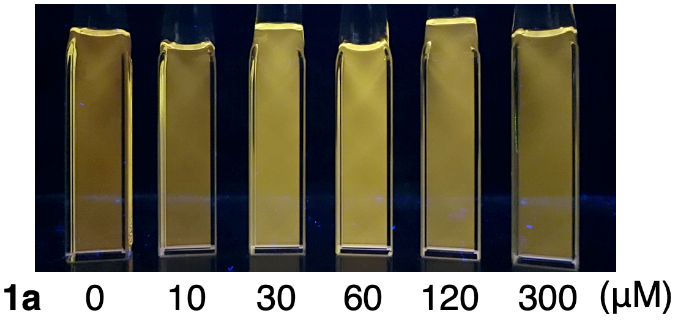

Figure S31. Photographic images of the CHCl$_3$ solutions (10 µM for [**3**]PF$_6$) with various amounts of **1a** under photoirradiation (λ_{ex} = 365 nm).

Modeling structure of **2**⊃[**3**]$^{+}$

The modeling structure was made up on the basis of their individual X-ray structures. The volume of the residual inner spaces in **2**⊃[**3**]$^{+}$ were estimated by the VOIDOO calculations. The alkyl chains of **2** were omitted in the model for clarity.

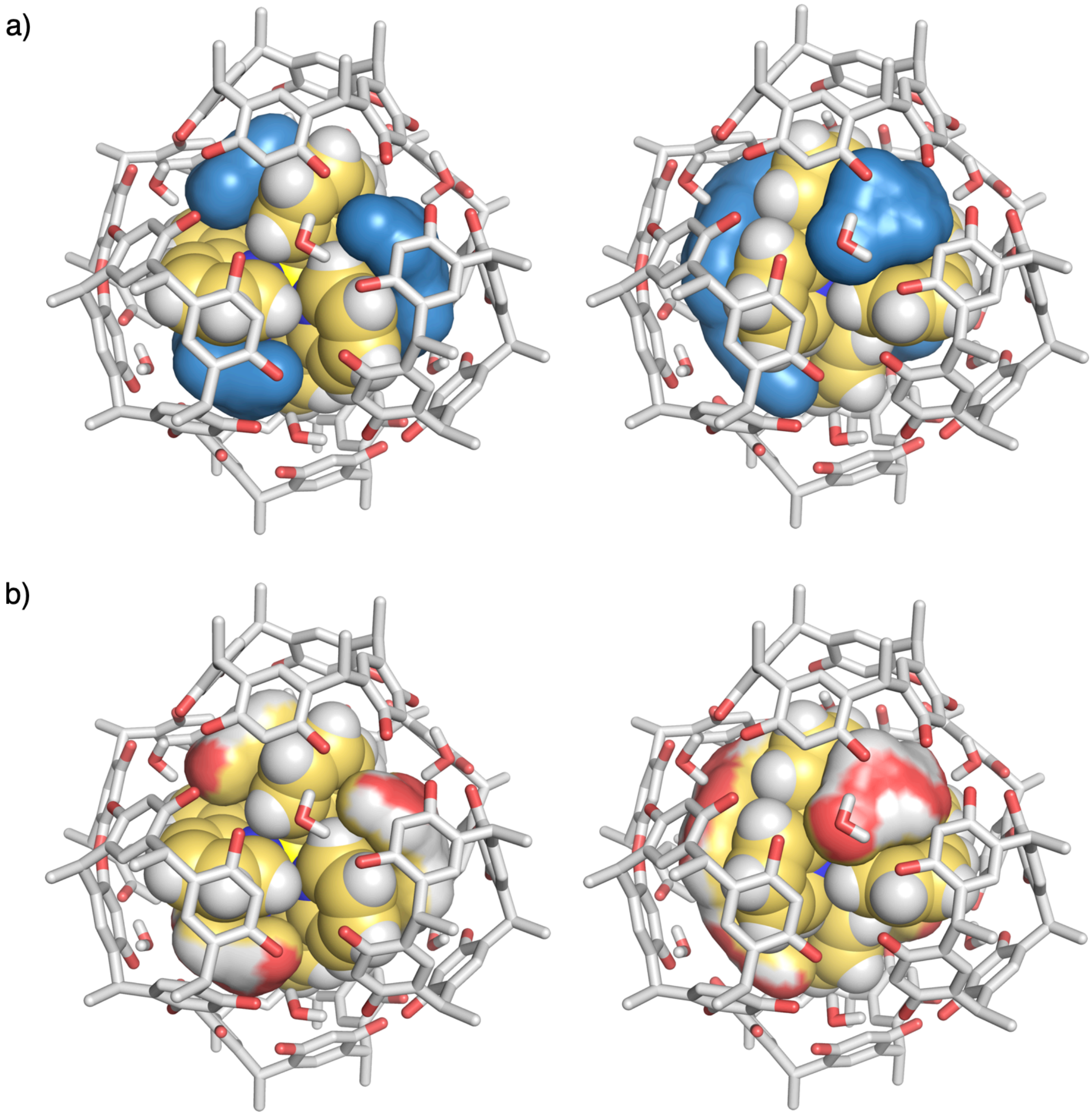

Figure S32. A modeling structure of **2**⊃[**3**]$^{+}$. H atoms and a counter anion were omitted for clarity. Hexameric capsule **2** is depicted by thick sticks, and Ir(III) complex cation [**3**]$^{+}$ is depicted by space-filling model: (left) front view, (right) back view. The inner spaces are shown with a) blue spheres and b) spheres with the same colors as the neighboring atoms. These modeling studies clearly show that the inner spaces are contacting with hydrophilic groups in the capsule framework.